JACS
JOURNAL OF THE AMERICAN CHEMICAL SOCIETY
pubs.acs.org/JACS
Article

# Revealing the Crucial Roles of Pore Interconnectivity between Zeolitic and Nonzeolitic Components in Enhancing Diffusion and Catalytic Efficiency of Industrial Zeolite-Based Catalysts

Yipu Xu, Peng Peng,* Hanlixin Wang, Hao Xiong, Zhaochao Xu, Xiao Chen, Yanpeng Li, Anmin Zheng, Yingxu Wei, Zifeng Yan,* Shutao Xu,* and Zhongmin Liu

Cite This: J. Am. Chem. Soc. 2025, 147, 18550−18562

Read Online

ACCESS | Metrics & More | Article Recommendations | Supporting Information

**ABSTRACT:** One of the utmost targets for catalysis research is to meet social needs in a profitable manner. Zeolitic and "nonzeolitic components" (such as silica, alumina, amorphous aluminosilicate, clay, etc.), as indispensable constituents of an industrial catalyst, both actively participate in industrial processes like polyolefin catalytic cracking and residue fluid catalytic cracking. Yet, the main research activities focus mainly on the diffusion behaviors of a single zeolitic or nonzeolitic component. In this work, the pore interconnectivity between zeolitic and nonzeolitic components to better ensure the diffusion and migration of reaction intermediate products in between was systematically studied by adopting a series of ZSM-5@meso-$SiO_2$ core−shell mesostructures as models to mimic industrially applied multicomponent zeolite-based catalysts with varying pore interconnectivities between the zeolitic (ZSM-5) and nonzeolitic components (meso-$SiO_2$). Their distinctive differences in the multiscale diffusion behaviors and structure-performance relationships represent the following three summarized scenarios: (1) micro/mesopore orientation, (2) spatial distribution of components, and (3) micro/mesoporous relative pore sizes thereof. These reveal that a well-connected micro/mesopore network can effectively accelerate interfacial diffusion and fully enhance the catalytic efficiency of the zeolitic component, highlighting the foundational functions of pore interconnectivity between zeolitic and nonzeolitic components in terms of the significance of the free migration of reactant species in between.

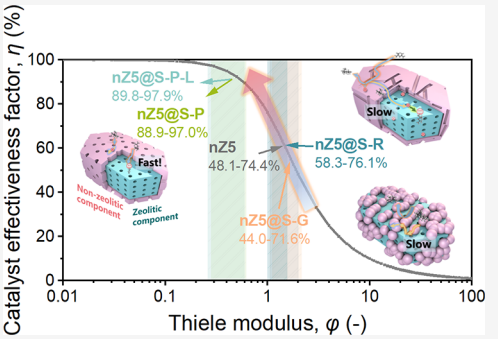


## INTRODUCTION

Owing to the unique crystalline microporous framework, finely tunable acid/base property, and excellent ion conduction ability, zeolites play pivotal roles in chemical manufacture,[1,2] environment recovery,[3,4] energy transition,[5] etc. Additionally, the intrinsic intracrystalline diffusion limitations within the narrow zeolite framework can be dramatically soothed via introducing secondary pore networks,[6−8] leading to enhanced catalytic efficiency.[9,10]

However, (hierarchical) zeolites alone cannot be directly utilized in actual industrial chemical processes.[11] Nonzeolitic components, such as silica, alumina, amorphous aluminosilicate, and clay, are also indispensable parts of the industrial catalysts as they fulfill rigorous requirements under harsh operational conditions (e.g., mechanical strength for fluidization, hydrothermal stability for extremely high temperature, poisoning/coking resistance for impurity-containing feedstock, etc.).[12−15] Except for the contributions to the above-mentioned mechanical and engineering aspects, these nonzeolitic components themselves are not inert spectators of some industrial catalytic processes but active participants. For the processes involving bulky reactants, such as polyolefin catalytic cracking (PCC) and residue fluid catalytic cracking (RFCC), two steps are needed: (I) preconversion of initial bulky reactants into intermediates (preliminary cracking step) via mesoporous nonzeolitic components and (II) conversion of intermediates into low-carbon and value-added products (deep cracking step) via zeolitic components.[1,16−18] Therefore, in order to coordinate both the preliminary and deep cracking steps for the "dual improvements" of both catalytic cracking conversion and low-carbon olefin selectivity, free migration of the intermediates in between zeolitic and nonzeolitic components should be ensured.

In view of mass transfer, such free migration of the intermediates is dependent on the pore interconnectivity between zeolitic and nonzeolitic components.[19] Although researchers have intensively studied the diffusion behavior within a single zeolitic or nonzeolitic component, reports on the influence of pore interconnectivity between zeolitic and

Received: January 6, 2025
Revised: May 14, 2025
Accepted: May 16, 2025
Published: May 26, 2025







https://doi.org/10.1021/jacs.5c00214
J. Am. Chem. Soc. 2025, 147, 18550−18562

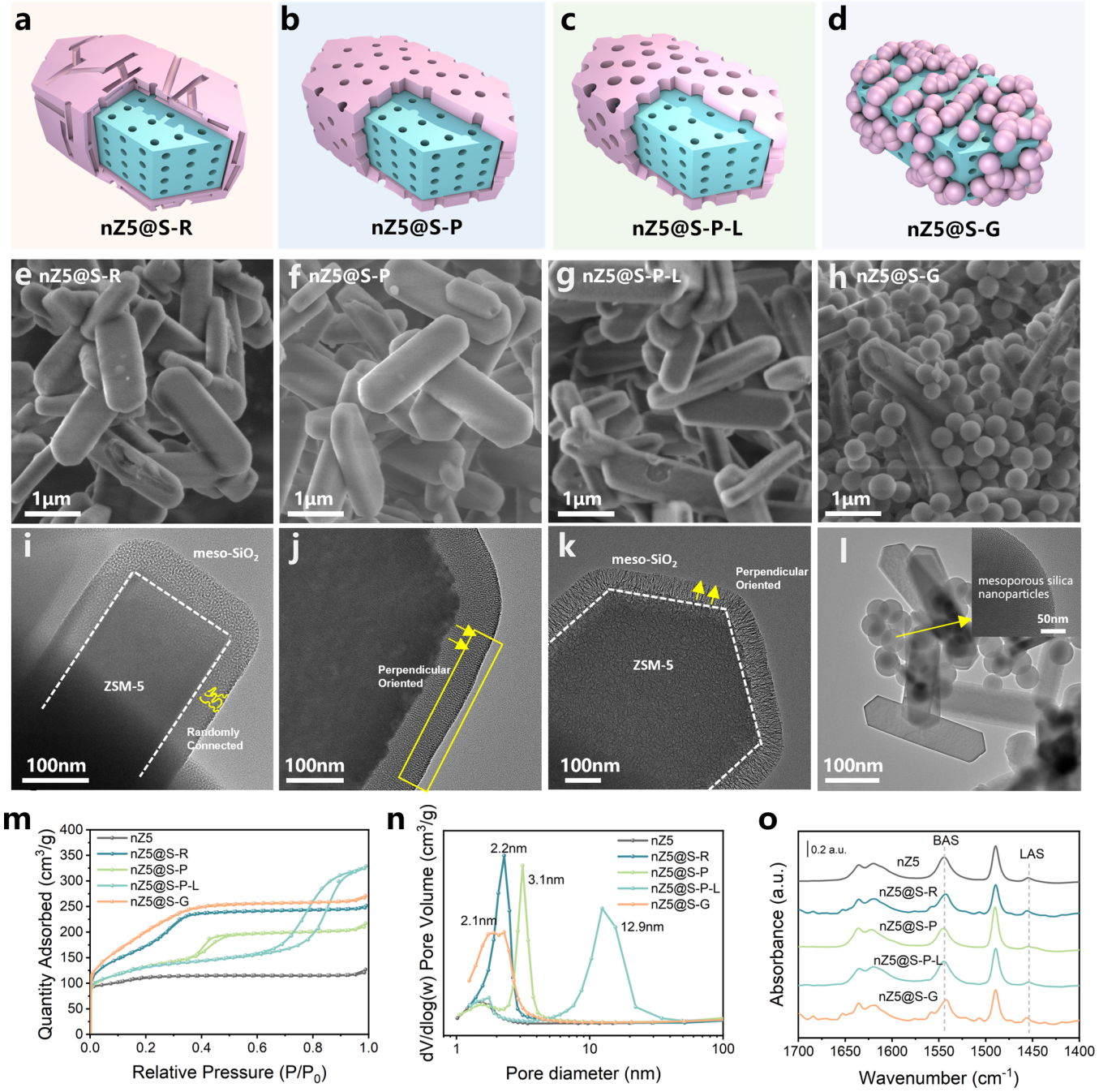


**Figure 1.** (a–d) 3D structure scheme of the ZSM-5@meso-$SiO_2$ core–shell mesostructures are illustrated schematically to facilitate visualization. The blue part represents zeolite components, and the pink part represents nonzeolite components. (e–h) SEM and (i–l) TEM images of ZSM-5 and ZSM-5@meso-$SiO_2$ core–shell mesostructures. The arrows indicate the connection between the micropores from the ZSM-5 core and the mesopores from the coating $SiO_2$ shells. (m) Nitrogen adsorption–desorption isotherms. (n) BJH pore size distribution curves. (o) IR spectra of model catalysts using pyridine as a probe molecule measured at 423 K (Py-IR).

nonzeolitic components on catalytic reaction are still scarce. Recently, several research groups have noticed that the pore structures and diffusion features of practical industrial catalysts strongly differ from their purely zeolitic counterpart due to the introduction of nonzeolitic components.[20−22] Song and co-workers[23] infer that the rate-determining step for industrial zeolite-based catalysts is not the intracrystalline diffusion within zeolite components but may be the diffusion at the interface between their zeolitic and nonzeolitic components. Our previous works also confirmed that the differences in macroscopic diffusion behaviors between the multicomponent catalyst and its zeolitic moiety.[24] However, understanding the added complexity of these multicomponent systems and the consequences for the structure-diffusion-reactivity relationships remains elusive in academic research. The entanglement of complex multiscale diffusion behaviors in multicomponent catalysts impedes the design of cost-effective industrial zeolite-based catalysts. Therefore, the changes in diffusion and catalytic efficiency caused by nonzeolitic components need to be mechanistically investigated. This is of utmost importance for the rational design of highly efficient zeolite-based catalysts at the industrial catalyst level. Nevertheless, it is still a challenge to



https://doi.org/10.1021/jacs.5c00214
J. Am. Chem. Soc. 2025, 147, 18550−18562

achieve a systematic and fundamental understanding of the influences of pore interconnectivity between zeolitic and nonzeolite components and their consequences on diffusion and catalyst efficiency, especially when directly relying on a real industrial catalyst. On the one hand, since the design and manufacture of the applied contemporary industrial catalysts still heavily rely on "trial and error,"[25] the empirical information based on them cannot always be generalized to other fabrication cases.[26] On the other hand, because of the entangled complexity of these multicomponent systems, the results are therefore challenging to decouple, making them sometimes unjustified.

Although it is still challenging to fully understand the migration and diffusion of guest molecules within real industrial catalysts, factors affecting pore interconnectivity between zeolitic and nonzeolitic components can still be figured out and summarized based on plenty of research and exploitation on them. Three key influential scenarios are listed herein: (1) Different pore orientations between microporous zeolitic and mesoporous nonzeolitic components, (2) different spatial distributions of mesoporous nonzeolitic components, and (3) relative pore size between microporous zeolitic and mesoporous nonzeolitic components.

In this work, the effects of pore interconnectivity between zeolitic and nonzeolitic components were systematically investigated via constructing a corresponding ZSM-5@meso-$SiO_2$ core−shell material as a model catalyst system, where the ZSM-5 core and the meso-$SiO_2$ shell served as zeolitic and nonzeolitic components, respectively. Each of the above factors affecting pore interconnectivity between zeolitic and nonzeolitic components had its own elaborated representative model catalyst system via a specific Stöber-based synthesis strategy. The distinctive pore interconnectivity of their respective elaborated representative model catalyst systems between the zeolitic (ZSM-5) and nonzeolitic components (meso-$SiO_2$) were confirmed by SEM, TEM, small-angle X-ray scattering (SAXS), and laser-hyperpolarized $^{129}$Xe (HP $^{129}$Xe) one-dimensional variable temperature nuclear magnetic resonance (1D VT NMR) and two-dimensional exchange spectroscopy NMR (2D EXSY NMR). Furthermore, the global diffusion and zeolitic portion diffusion behaviors of the model multicomponent catalysts were investigated by intelligent gravimetric analysis (IGA) and time-resolved in situ Fourier transform infrared spectroscopy (time-resolved in situ FTIR). The differences in the macroscopic diffusion behaviors and structure-performance relationship during catalytic cracking reactions in the model catalysts were quantitatively established.

## RESULTS AND DISCUSSION

**Construction of ZSM-5@meso-$SiO_2$ Multicomponent Model Catalysts.** A short *b*-oriented ZSM-5 nanosheet was selected as the core since it can effectively alleviate the intracrystalline diffusion resistance at the zeolitic level (SEM and TEM images in Figure S6a).[27−29] Based on four different Stöber-based synthesis strategies, intimately contacted meso-$SiO_2$ shells, different from the mechanical mixture, were overgrown on the surface of *b*-oriented ZSM-5 nanosheets.[30] For mimicking the three scenarios of pore interconnectivity, three types of core−shell samples were adopted. (1) Orientation between the microporous core and mesoporous shell is either well connected (nZ5@S-P, Figure 1b) or randomly connected (nZ5@S-R, Figure 1a). (2) The meso-$SiO_2$ shell is either uniformly coated (as shown in nZ5@S-R, Figure 1a) or randomly dispersed (as shown in nZ5@S-G, Figure 1d) on the surface of the ZSM-5 core. (3) The mesopore diameter of the meso-$SiO_2$ shell is confined to smaller (nZ5@S-P, ∼3.1 nm) or larger (nZ5@S-P-L, ∼12.9 nm, Figure 1c). The different morphologies and pore distributions for the four ZSM-5@meso-$SiO_2$ samples are assured by their different Stöber-based synthesis strategies,[31,32] which has·been illustrated as Figure S1 and its corresponding notes in the Supporting Information. For more information on preparation and physicochemical characterizations of these samples, see the Supporting Information (Figures S6−S9: Supplementary SEM images and magnified TEM images; Table S1: Textural properties and acidity data of the ZSM-5 nanosheet and the four ZSM-5@meso-$SiO_2$ samples).

*Scenario I*, i.e., different pore orientations in between microporous zeolitic and mesoporous nonzeolitic components were represented by nZ5@S-R and nZ5@S-P samples where alignment of the $SiO_2$ mesopores is either more perpendicular (Figure 1b) or less (Figure 1a) to the surface of the ZSM-5 nanosheet, respectively. By comparing the TEM images of nZ5@S-P (Figure 1j, magnified TEM images in Figure S8) and nZ5@S-R (Figure 1i, magnified TEM images in Figure S7), the mesopore of the shell for nZ5@S-P is indeed more perpendicular to the micropore of the ZSM-5 nanosheet, while the core and shell of the nZ5@S-R sample are not fully connected due to randomly oriented micro- and mesopores. The magnified TEM images of nZ5@S-R and nZ5@S-P are presented separately as Figures S7 and S8 of the Supporting Information. Such differences in the alignment of $SiO_2$ mesopores in between Z5@S-P and nZ5@S-R samples are also in accordance with the SAXS pattern shown in Figure S5 of the Supporting Information. The single scattering peak at the $q$ value of 0.53 $nm^{-1}$, inferring the perpendicular stretch to the micropore of ZSM-5, exclusively appears in the nZ5@S-P sample but is absent in Z5@S-R. Additionally, for the nZ5@S-P sample, its nitrogen adsorption−desorption isotherm (Figure 1m) displays parallel adsorption and desorption branches, indicating typical open and channel-like mesopores.[33] Besides, the SEM images of both samples (Figure 1e,f) exhibit that the *b*-oriented ZSM-5 zeolite nanosheet is coated by a uniform mesoporous $SiO_2$ shell. The pore size distribution curves show that the mesopores are highly concentrated at a pore size of c.a. 2−3 nm (BJH pore size distribution curves in Figure 1n). The integrated differential phase contrast (iDPC) scanning transmission electron microscopy (STEM) images (Figure S10) confirm that the incorporation of meso-$SiO_2$ does not influence the pore mouth or surface defects. *Scenario II*, i.e., different spatial distributions of mesoporous nonzeolitic components were represented by the nZ5@S-R and nZ5@S-G samples, where the mesoporous $SiO_2$ is either a uniformly coated surface of the ZSM-5 nanosheet (Figure 1a) or just deposited on it as mesoporous spheres (Figure 1d), respectively. The SEM (Figure 1e) and TEM (Figure 1i) images of the samples exhibit a mesoporous $SiO_2$ shell uniformly coating the surface of the *b*-oriented ZSM-5 zeolite nanosheet in the nZ5@S-R sample. In contrast, the TEM images (Figures 1l and S6e) and SEM images (Figures 1h and S6e) of the nZ5@S-G sample show that mesoporous $SiO_2$ submicrometer spheres are either around the surface of the ZSM-5 core or loosely packed in the empty space among the coffinlike ZSM-5 crystals. *Scenario III*, i.e., the relative pore size between microporous zeolitic and mesoporous nonzeolitic components was represented by nZ5@S-P with a mesopore size of ∼3.1 nm and nZ5@S-P-L of ∼12.9 nm illustrated by each of their BJH pore size distribution curves


https://doi.org/10.1021/jacs.5c00214
J. Am. Chem. Soc. 2025, 147, 18550−18562

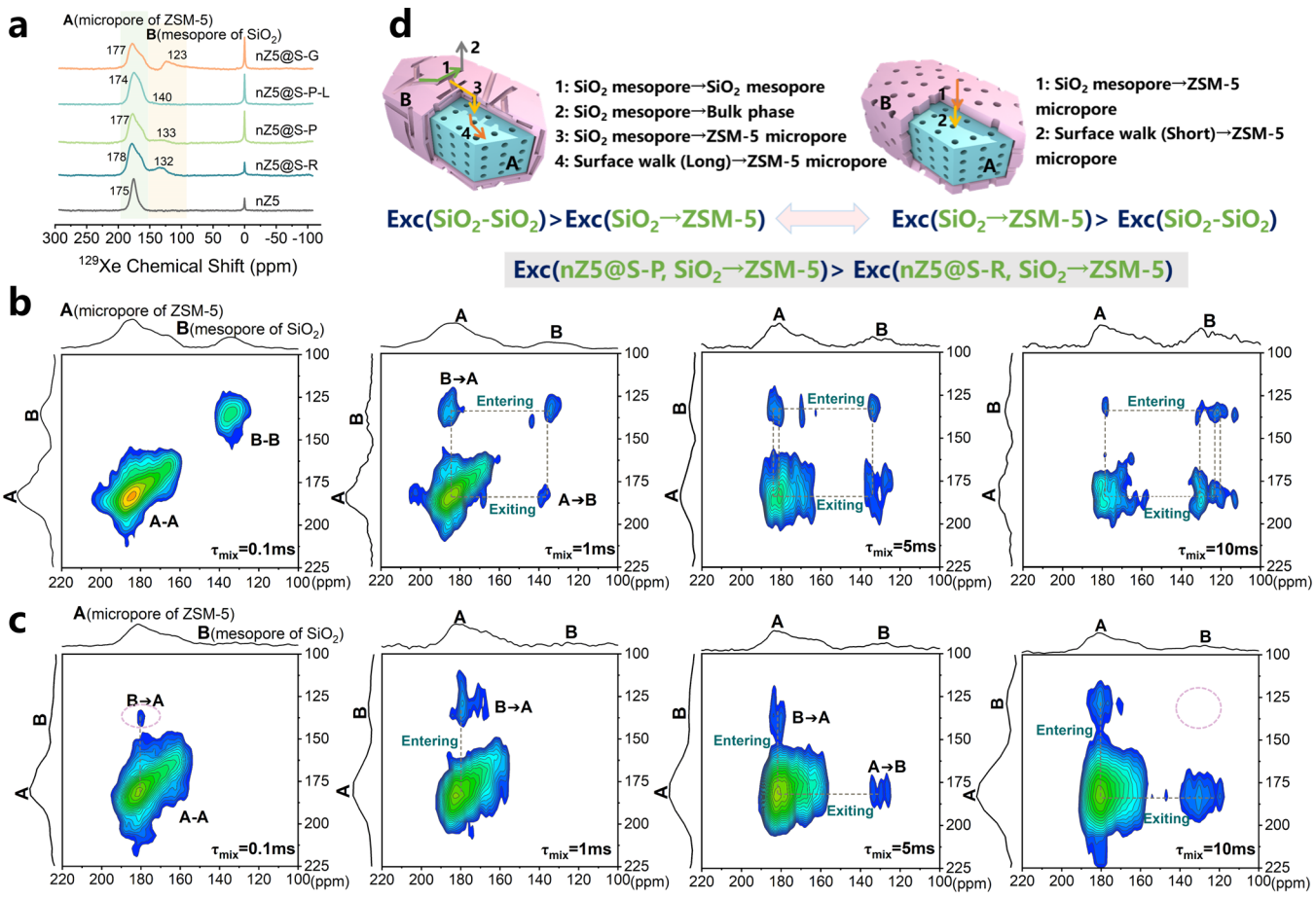


**Figure 2.** (a) HP $^{129}$Xe NMR spectra of Xe adsorbed in ZSM-5 and ZSM-5@meso-$SiO_2$ model catalysts at 143 K. (b, c) HP $^{129}$Xe 2D EXSY NMR spectra of Xe adsorbed in (b) nZ5@S-R and (c) nZ5@S-P at 133 K, respectively. (d) Diffusion pathway diagram of nZ5@S-R (left) and nZ5@S-P (right).

(Figure 1n) and magnified TEM images (Figures 1c and S9). The above results verify that the four ZSM-5@meso-$SiO_2$ core−shell materials can indeed effectively represent the above-mentioned three scenarios summarizing the factors affecting pore interconnectivity between zeolitic and nonzeolitic components.

To draw a more systematic conclusion, the model catalysts need to be simplified from real industrial catalysts and subjected to precision control. This study mainly focuses on the impact of the pore interconnectivity between components. To highlight this effect, other potential influencing factors, such as the acidity of nonzeolitic components and aluminum migration, are intentionally excluded. Due to the mild synthetic conditions of the adopted Stöber-based synthesis strategies, the endowment of meso-$SiO_2$ does not lead to apparent aluminum migration that might be observed in industrial catalysts,[13,14] which can be confirmed by the $^{27}$Al MAS NMR spectra (Figure S14c) and STEM-mapping (Figure S15). Additionally, supplementary experiments have demonstrated that the post-treatment $SiO_2$ coating synthesis conditions do not cause any significant alterations to the ZSM-5 zeolitic component (Figures S11 and S12 and the following discussion in the Supporting Information). Besides, the pyridine absorbed IR spectra (Figure 1o), $NH_3$-TPD profiles (Figure S13), and corresponding acid site quantification data (Table S1) further confirm that the incorporation of the meso-$SiO_2$ shell does not alter the inherited acid properties of the ZSM-5 core, while the $^{29}$Si MAS NMR (Figure S14a,b), $^{27}$Al MAS NMR (Figure S14c), and $^{1}$H MAS NMR spectra for all model catalysts (Figure S14d) indicate that there is no significant change of ZSM-5 framework aluminum after the introduction of the $SiO_2$ process. At this stage, we have successfully constructed three categories of model catalysts, each representing distinct pore interconnectivity characteristics: different micro/mesopore orientation (nZ5@S-P and nZ5@S-R), different spatial distribution of components (nZ5@S-R and nZ5@S-G), and different micro/mesoporous relative pore sizes (nZ5@S-P and nZ5@S-P-L). Throughout the synthesis process, the pore structure is the primary regulatory factor, while other physicochemical properties remained largely consistent across the model samples. Consequently, considering the closest comparability in both porous architecture and acidic properties, the optimal samples, namely, nZ5@S-R, nZ5@S-P, nZ5@S-P-L, and nZ5@S-G, have been used as model catalysts to determine the impact of pore interconnectivity between components, and the characteristics of the pore network, including diffusion properties, are characterized in detail.

**Identification of Multicomponent Hierarchical Pore Network Connectivity.** To gain a deeper insight into the pore interconnectivity of the ZSM-5@meso-$SiO_2$ core−shell meso-structures, HP $^{129}$Xe 1D VT NMR and 2D EXSY HP $^{129}$Xe NMR techniques were adopted for identifying the exchange rate and diffusion path of probe molecules in between zeolitic and nonzeolitic components (Figure 2). HP $^{129}$Xe NMR is a powerful tool to explore the exchange rate during the rapid


https://doi.org/10.1021/jacs.5c00214
J. Am. Chem. Soc. 2025, 147, 18550−18562

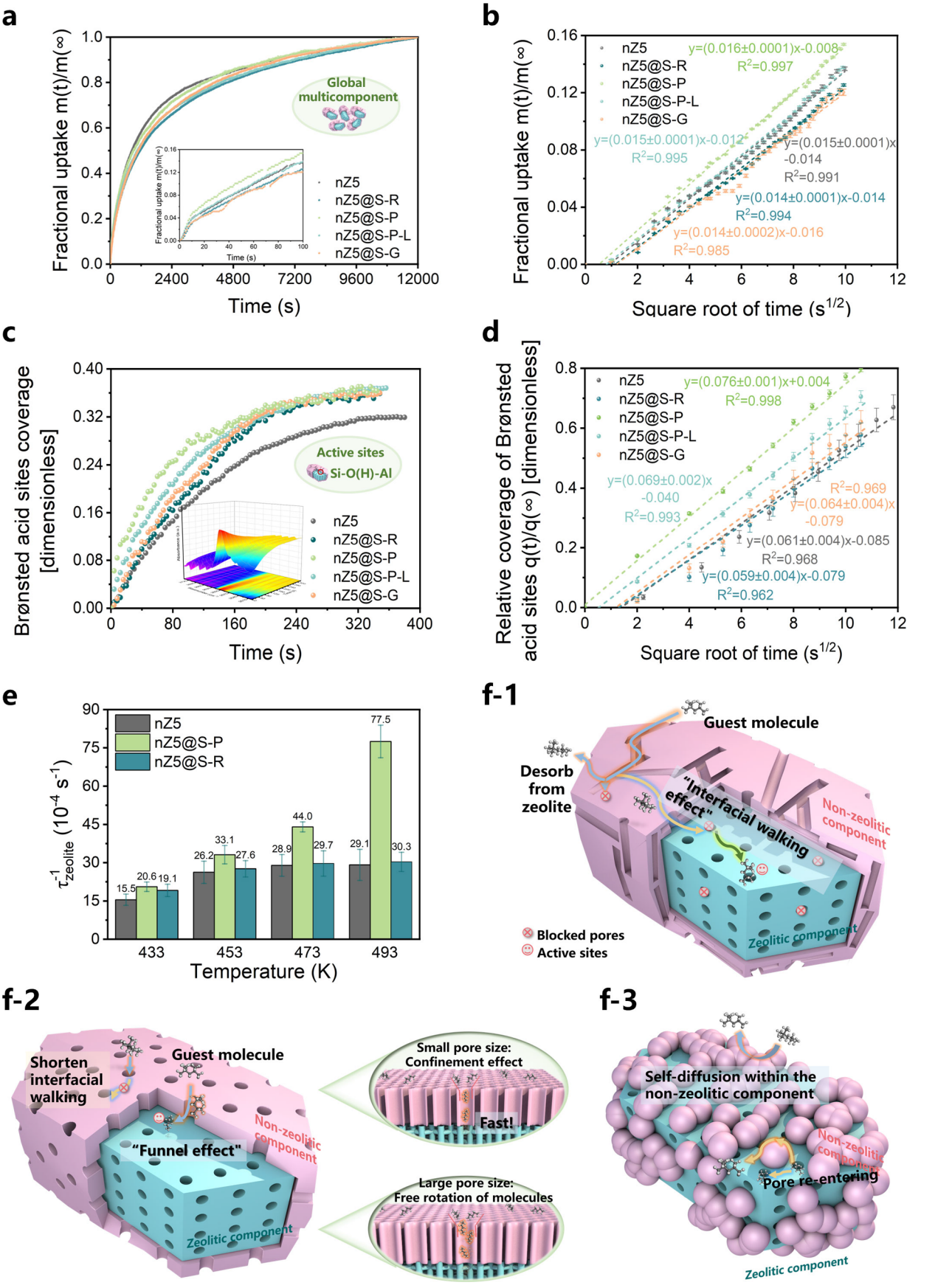


**Figure 3.** (a, b) Isooctane uptake curves for model catalysts measured by IGA technique at 473 K: (a) normalized relative uptake as a function of time and (b) global fractional uptake as the square root of time. (c, d) Isooctane uptake curves of model catalysts measured by time-resolved rapid-scan in situ FTIR technology at 473 K: (c) coverage of Brønsted acid site as a function of time (inset is the absorbance variation of IR spectra in the Si−O(H)-



https://doi.org/10.1021/jacs.5c00214
J. Am. Chem. Soc. 2025, 147, 18550−18562

**Figure** 3. continued

Al region of nZ5 catalyst as a function of time as an example) and (d) normalized relative coverage of Brønsted acid sites as a function of square root of time. The characteristic diffusion time constants $\tau_{global}^{-1}$ and $\tau_{zeolite}^{-1}$ can be obtained from the slope of linear in (b) and (c) (cf. Supporting Information), which represent the macroscopic diffusion behaviors of the global model catalyst and its zeolitic moiety, respectively. (e) Relationship between temperature and zeolitic component diffusion time constant $\tau_{zeolite}^{-1}$ obtained from isooctane uptake time-resolved in situ FTIR experiments. (f) Proposed diffusion pathway for the mass transport of isooctane molecule during the interface of zeolitic and nonzeolitic component model catalyst: (f-1) pore orientation between the nonzeolite component and zeolite component is not well-connected, (f-2) zeolitic micropore is well-oriented to the nonzeolitic mesopore, and (f-3) spatial distribution of nonzeolitic components is randomly dispersed around the zeolitic component.

exchange condition with high sensitivity by detecting the differences the chemical shift reflect.[34−36] Besides, the spin exchange optical pumping method, by which alkali metal electron spins toward the $^{129}$Xe nuclear spins can be polarized, can effectively reduce the nuclear relaxation time and improve the detection sensitivity.[34,37] The exchange of xenon atoms between different pore environments leads to time-dependent averaging of chemical shifts, which can be analyzed using EXSY NMR or VT NMR. The peak at 0 ppm is assigned to xenon in the gas phase, while the other two peaks at ∼175 and 120−140 ppm contributed to the adsorbed Xe in the ZSM-5 micropore and the $SiO_2$ mesopore, respectively (Figures 2a and S16). Since the chemical shift of $^{129}$Xe includes various interactions between xenon atoms and pore materials, the chemical shift difference ($\Delta\delta$) of Xe between the core and the shell can be used to reflect the exchange rate under rapid exchange conditions.[34,38] This correlation is rooted in the exchange regime of nuclear spins, which can be described using the Bloch-McConnell equations for two-domain exchange systems.[39,40] The various values of the chemical shift observed for many different structures allowed us to establish a relationship between the chemical shift and the exchange rate via the mean free path of a Xe atom diffusing in the pores. When in the slow-exchange regime, the xenon atoms remain in their respective environments long enough for distinct chemical shifts to be observed, a faster exchange rate results in xenon rapidly migrating between two domains, averaging the Xe-Xe chemical shifts. For the same ZSM-5-contained multicomponent materials, a smaller $\Delta\delta$ value indicates faster xenon exchange between the mesopores and micropores. Sample nZ5@S-P-L reveals a narrower and more symmetric peak at 174 ppm (ZSM-5 signal) and an additional signal at 140 ppm (assigned to the unrestricted rapid exchange in larger mesopores). Besides, its $\Delta\delta$ (34 ppm) is the lowest among all of the samples. Such results indicate the highest xenon exchange rate between micro- and mesopores. In addition, the $\Delta\delta$ of two domains in sample nZ5@S-G is 54 ppm, indicating its slower exchange rate compared with the uniformly coated nZ5@S-P and nZ5@S-R samples. This may be because the Xe exchange chiefly happens within the mesoporous shell, and only a small portion of Xe exchanges occur between the core and the shell. For the two uniformly coated core−shell samples, the $\Delta\delta$ of nZ5@S-P is 2 ppm smaller than that of nZ5@S-R, inferring their differences in pore interconnectivity and diffusion behaviors. In order to unravel the detailed xenon dynamic processes and motion pathways of the above two samples, 2D EXSY HP $^{129}$Xe NMR with mixing times ($\tau_{mix}$) of 0.1, 1, 5, and 10 ms at 133 K was adopted (Figure 2b,c). 2D EXSY NMR spectroscopy is a powerful tool employed to provide dynamic processes about the motion pathways of xenon between different sites. By using the continuous-flow technique, hyperpolarized Xe can be continuously delivered to the sample allowing the recording of 2D exchange spectra and collection of information on the interconnectivity of the hierarchical pore orientation. The off-diagonal cross peaks in 2D EXSY HP $^{129}$Xe NMR infer the existence of xenon exchange between the microporous ZSM-5 core (A) and the mesoporous $SiO_2$ shell (B) with the given mixing time (denoted as A−B), while the peaks shown at the diagonal are assigned to the self-correlation within the core (denoted as A−A) and/or the shell (denoted as B−B). At a short mixing time ($\tau_{mix}$) of 0.1 ms, the absence of off-diagonal cross peaks in nZ5@S-R reveals that there is no exchange between its core and shell. This phenomenon is consistent with the results of TEM and SAXS, further suggesting undesired pore interconnectivity, allowing for multiple collisions and exchanges of Xe in the $SiO_2$ mesopores. The cross peaks are more intensive with the increase of $\tau_{mix}$ in the nZ5@S-R sample, indicating its enhanced "A−B" domain xenon exchange. The result shows that the rate of exchange of xenon between $SiO_2$−$SiO_2$ (B−B) domains is faster than that between $SiO_2$-ZSM-5 (B−A) domains. This indicates that $^{129}$Xe exchange between mesopores occurs faster, suggesting that mesopore connectivity is superior to micropore-mesopore connectivity. In contrast, for the sample with well-interconnected micro- and mesoporosity (nZ5@S-P), only a weak cross-peak signal is observed with no signals attributed to mesopore self-correlation at a $\tau_{mix}$ of 0.1 ms. As $\tau_{mix}$ increases, even though the cross-peak signal becomes more pronounced, there is still no mesopore self-correlation signal even after 10 ms, indicating its enhanced "A−B" domain xenon exchange rate. This kind of exchange is always superior to that of "B−B" domains. These results unambiguously confirm the distinctive diffusion paths and behaviors of the two samples.

Based on the $^{129}$Xe NMR results, possible diffusion paths for the samples with different micro/mesopore interconnectivities are summarized (Figure 2d). For the sample where the relative orientations of micro/mesopores are random (nZ5@S-R), although its interconnectivity between micro- and mesoporous structures is inferior, the interconnectivity of mesoporous $SiO_2$ is still greatly improved. In this case, the guest molecules located at the meso-$SiO_2$ shell (nonzeolitic component) may leave from the sample system after a long period of mesopore diffusion, and only a small portion of guest molecules can continue to diffuse along the interconnected meso-$SiO_2$ and/or external surface of the zeolite until they find an interconnected entrance to enter the microporous zeolitic component. Such a process obviously results in a greatly increased diffusion path length, leading to a lower Xe exchange rate. This process is defined as "interfacial walking effect." On the contrary, owing to the well-connected micro- and mesoporous channels (nZ5@S-P), not only can the possibility of guest molecules entering the zeolitic channels be effectively raised, but also the diffusion along the zeolitic external surface is shortened, and even the diffusion entities within the mesoporous shell can be emptied due to the greatly decreased path length (showed in Figure 2c with $\tau_{mix}$ of 5 and 10 ms), thereby accelerating the Xe exchange rate between the microporous core and the mesoporous shell.



https://doi.org/10.1021/jacs.5c00214
J. Am. Chem. Soc. 2025, 147, 18550−18562

**Relating Pore Interconnectivity to Diffusion in Multicomponent Model Catalysts.** The above characterization and identification of pore interconnectivity of the ZSM-5@meso-$SiO_2$ core−shell mesostructures results confirm the significant differences in the arrangement and orientation between their microporous zeolitic core and mesoporous nonzeolitic shell. In order to fully analyze how different arrangements and orientations affect the diffusion properties of the ZSM-5@meso-$SiO_2$ core−shell materials, two techniques, i.e., IGA and time-resolved in situ FTIR analysis, were adopted to investigate the macroscopic diffusion behaviors of the global model catalyst and its zeolitic moiety, respectively (Figure 3). In order to avoid the inappropriate estimation of diffusion path length ($L$) which can further cause errors in the estimation of effective diffusivity ($D_{eff}$), the diffusion time constant ($\tau$, present as $\tau^{-1}$ thereafter for comparison), which is a function of both the effective diffusivity and the diffusion path length ($\tau^{-1} = D_{eff}/L^2$), is calculated as the descriptor for evaluating diffusion properties in this work. The quantification of characteristic diffusion time constant $\tau^{-1}$ can be obtained from the slope of linear portion of the fractional uptake versus square root of time plots (Figure 3b,d), which is valid for the initial uptake for particles of arbitrary shapes (detailed quantification information cf. Supporting Information 1.4.):

$$\frac{q(t)}{q(\infty)} = \frac{2}{\sqrt{\pi}}\sqrt{\frac{Deff}{L^2}}\sqrt{t} = \frac{2}{\sqrt{\pi}}\sqrt{\frac{t}{\tau}}$$

where $q(t)$ and $q(\infty)$ are the uptake of probe molecule at time $t$ and at equilibrium, respectively. 2,2,4-Trimethylpentane (isooctane) was chosen as a probe molecule not only because it is a typical intermediate after bulky molecules (such as polyolefin or residual oil) precracking within the nonzeolitic component but also due to its kinetic diameter (0.62 nm) being larger than the pore openings of ZSM-5 zeolite (0.55 nm).

The global diffusion behaviors of the model multicomponent catalysts measured by IGA and the corresponding diffusion time constant reciprocal (indexed as $\tau_{global}^{-1}$) at 473 K are shown in Figure 3a,b, Tables S2,and 1. The isooctane global fractional uptake curves show that $\tau_{global}^{-1}$ of the samples increases in the following order: nZ5@S-G < nZ5@S-R < nZ5 < nZ5@S-P-L < nZ5@S-P. At the initial stage of the diffusion process, the apparent uptakes of isooctane for samples nZ5@S-P-L and nZ5 are quite close and lower than those of nZ5@S-P, while nZ5@S-G and nZ5@S-R show a slower diffusion rate than nZ5, indicating that introducing mesopores into microporous (zeolite) structures does not always lead to enhanced diffusion properties. Previous works by various research groups have demonstrated that for the single zeolitic component only, introducing mesostructures does accelerate intracrystalline diffusion.[41−44] Considering that the zeolitic component of model samples, a *b*-oriented ZSM-5 nanosheet which increased intracrystalline diffusion along the shortened *b*-axis, has been demonstrated,[27] however, such a scenario is not always the case for the multicomponent catalyst. Our results for model multicomponent catalysts indicate that not all samples experience an increase of diffusion properties ($\tau_{global}^{-1}$: nZ5@S-P > nZ5@S-P-L> nZ5). Instead, such rates of some mesoporous samples are even slower than that of their single-component zeolitic counterparts ($\tau_{global}^{-1}$: nZ5@S-G < nZ5@S-R < nZ5). Such phenomena reflect the effects of mismatched interconnectivity between micro- and mesoporous interfaces. The results show that under multicomponent catalyst circumstances, the nonideal pore interconnectivity, such as mismatched spatial distribution and/or pore orientation between the zeolitic and nonzeolitic components, can deteriorate the full enhancement of diffusion properties owing to the hierarchical zeolite. This is in good accordance with our previous works.[24] Another interesting phenomenon is that the sample with a larger size of mesoporous shell does not always lead to a faster diffusion rate ($\tau_{global}^{-1}$: nZ5@S-P > nZ5@S-P-L). This may be because the mesoporous shell with a smaller size has a confined space, which could provide a "hyperloop-like diffusion" phenomenon of long-chain molecules.[45] Its confined space might restrict the degree of freedom for diffusion in mesopores, reducing the disorder and forcing the molecules to diffuse in an orderly manner, thereby promoting transport.[46]

In order to further explore how the interconnectivity of the microporous core and mesoporous shell affects the diffusion properties of ZSM-5, time-resolved in situ infrared spectroscopy analysis was applied. In the ZSM-5@meso-$SiO_2$ composite catalyst, the chief active sites for the deep cracking in the bulky molecules involved processes like PCC or RFCC are Brønsted acid sites, which originated from bridged hydroxyl groups (Si−O(H)-Al) on the ZSM-5 framework.[16,47] Thus, technology can be recruited as a clue to track the exclusive diffusion property of ZSM-5 core when the meso-$SiO_2$ shell coexists (see the dynamic process as Figure S2 in the Supporting Information).[48] Direct quantitative measurements of the diffusion property toward the ZSM-5 core are shown in Figure 3c,d, which were performed on the basis of the coverage of Si−O(H)-Al (IR signal at about 3610 $cm^{-1}$) as a function of time. A linear relationship is obtained by plotting the fractional coverage of Si−O(H)-Al versus the square root of time (Figure 3d). The corresponding diffusion time constant reciprocal, which is indexed as $\tau_{zeolite}^{-1}$, is summarized in Table 1. All tests have been repeated three times to obtain the average diffusion data and error bounds; the repeated experiments and fitting procedure are provided in Figures S17 and S18. The summary of repeated experiments results is listed in Table S3 and Figure S19. Statistically speaking, the nZ5@S-P sample exhibits a statistically significant enhancement in the diffusion performance. The samples nZ5, nZ5@S-R, and nZ5@S-G are statistically indistinguishable within the current experimental resolution. This may be attributed to the subtle structural differences among these three samples, which infer that under the industrial catalyst production conditions represented by samples nZ5@S-R and nZ5@S-G, the introduction of nonzeolitic components does not exhibit statistically significant effects on the diffusion properties of the zeolitic component itself exemplified by sample nZ5. Therefore, our discussion mainly focuses on the differences between the nZ5@S-P sample and the other samples. For the case where the micro- and mesopores are well connected (nZ5@S-P), its $\tau_{zeolite}^{-1}$ ($44.0 \times 10^{-4}$ $s^{-1}$) is approximately 1.5 times that for

**Table 1. Diffusion Time Constants of Isooctane Uptake Curves (Figure 3b,d) for Model Catalysts Calculated from IGA ($\tau_{global}^{-1}$) and Time-Resolved In Situ FTIR Technology ($\tau_{zeolite}^{-1}$)**

| sample | $\tau_{global}^{-1}$ ($10^{-4}$ $s^{-1}$) | $\tau_{zeolite}^{-1}$ ($10^{-4}$ $s^{-1}$) |
|---|---|---|
| nZ5 | 1.74 ± 0.07 | 28.9 ± 4.3 |
| nZ5@S-R | 1.52 ± 0.04 | 29.7 ± 5.0 |
| nZ5@S-P | 2.04 ± 0.05 | 44.0 ± 2.0 |
| nZ5@S-P-L | 1.77 ± 0.05 | 37.5 ± 3.2 |
| nZ5@S-G | 1.45 ± 0.09 | 32.1 ± 4.5 |


https://doi.org/10.1021/jacs.5c00214
J. Am. Chem. Soc. 2025, 147, 18550−18562

sample nZ5@S-R ($29.7 \times 10^{-4}$ $s^{-1}$). Compared with the randomly interconnected counterpart, the well-interconnected micro- and mesopores can significantly reduce the diffusion barrier between the components, showing that when the pore orientation of nonzeolite components is interconnected with zeolite components, the surface barrier for intermediates diffusing into the zeolite component is significantly reduced, showing great advantages in improving the accessibility of active-sensitive sites such as Brønsted acid sites. Interestingly, when the ZSM-5 micropore is well-oriented to the $SiO_2$ mesopore, as shown in nZ5@S-P, its diffusion constant can even exceed its single-component zeolitic counterpart of nZ5@S-P ($44.0 \times 10^{-4}$ $s^{-1}$) which is 1.52 times higher than that of ZSM-5 ($28.9 \times 10^{-4}$ $s^{-1}$), and that of nZ5@S-P-L ($37.5 \times 10^{-4}$ $s^{-1}$) is also higher than that of ZSM-5. Theoretically, coating an inert shell will inevitably block some zeolitic micropores, so the diffusion upper limit of core−shell multicomponent catalysts might be the same as that of ZSM-5. However, considering that the adopted $\tau_{zeolite}^{-1}$ exclusively reflects the diffusion properties of ZSM-5 and that the influence of diffusion in the mesoporous structure in $SiO_2$ has been ruled out, the enhanced diffusion rate of the ZSM-5 component clearly reveals that the pore interconnectivity in between zeolitic and nonzeolitic components has a significant promotional effect on the diffusion properties of ZSM-5. Considering the truncated diffusion pathways obtained from HP $^{129}$Xe NMR, the highest $\tau_{zeolite}^{-1}$ of the nZ5@S-P sample infers that its uniformly coated meso-$SiO_2$ shell that is well-connected to microporous ZSM-5 core may act as a "funnel" to directly pump the adsorbed guest molecules into the microporous ZSM-5 core by accelerating the interface diffusion between the two components.[46] Kärger and co-workers defines it as the contribution of the "transport pores," and their determination on already "simple" external surfaces is far from being trivial.[49,50] For the case where meso-$SiO_2$ is randomly dispersed (i.e., nZ5@S-G), its $\tau_{zeolite}^{-1}$ is much lower than that of the uniformly coated nZ5@S-P sample ($32.1 \times 10^{-4}$ vs $44.0 \times 10^{-4}$ $s^{-1}$), even similar to that of single-component ZSM-5 ($28.9 \times 10^{-4}$ $s^{-1}$). Since meso-$SiO_2$ partially covered the ZSM-5 surface, some guest molecules can still directly interact with the zeolitic component, and a great extent of guest molecules tend to diffuse within or on the surface of nonzeolite components following the diffusion processes mentioned above. Consistent with the IGA results, the sample with a lower mesoporous shell size exhibits higher diffusion property (nZ5@S-P, $\tau_{zeolite}^{-1}$: $44.0 \times 10^{-4}$ $s^{-1}$) than its larger mesoporous shell counterpart (nZ5@S-P-L, $\tau_{zeolite}^{-1}$: $37.5 \times 10^{-4}$ $s^{-1}$). As a direct consequence, the mesopore diameter of the overlayer is crucial for the transport process of the multiporous channels. This may be because the narrower pore size (2−3 nm) restricts the free rotation of isooctane macromolecules in the pores, so they can arrive at the interface with minimal energy. Also, its confined space might be closely related to the diffusion paths inside the complex structure of the surface pore mouths and the shapes of the guest molecules. This result again shows the importance on the compatibility of the microporous core and mesoporous shell, inferring that additionally introduced mesoporous structures do not always lead to higher diffusion property, and only the optimized pore size of micro- and mesostructures can effectively improve mass-transfer efficiency, which is consistent with some previous works done by Su and co-workers[51,52] A well-connected micro/mesopore network can effectively accelerate the interfacial diffusion, even exceeding its single-component zeolitic counterpart.

Based on HP $^{129}$Xe NMR, IGA, and time-resolved in situ FTIR results above-mentioned, the role of pore interconnectivity during diffusion at the interface of zeolitic and nonzeolitic components is discussed as follows. As illustrated in Figure 3f, mass transport within the multicomponent catalyst likely involves a combination of the zeolitic diffusion and interface diffusion between zeolitic and nonzeolitic components.[23,53] When the pore orientation of ZSM-5@meso-$SiO_2$ core−shell mesostructure is poorly connected (Figure 3f-1), the micropores at the zeolite's external surface are partially blocked, requiring guest molecules to diffuse within the nonzeolitic components or along the zeolite's surface, thereby extending the diffusion time. This "interfacial walking effect,", as previously discussed (Figure 2d), could be minimized by reducing the nonzeolitic component coverage on the zeolite surface. Furthermore, due to the prolonged mesopore diffusion path, the global diffusion property may not accurately represent the real diffusion rate into active sites. Distinguishing whether diffusion resistance arises from multiscale pore system connectivity or single-component contributions remains challenging. Here, time-resolved in situ FTIR technology offers valuable insights into distinguishing the diffusion contributions from the zeolitic components within multiscale pore systems. When the zeolitic micropores are well-oriented to nonzeolitic mesopores (Figure 3f-2), the interface diffusion could be accelerated. As guest molecules diffuse from the gas phase into micropores, the nonzeolitic mesopores can act as a "funnel" to directly pump the enriched guest molecules into the zeolitic micropores, thereby accelerating the interface diffusion between two components. This enhancement may be due to the gradual loss of entropy upon collision with the nonzeolitic mesopores, increasing the sticking probability.[46] Additionally, the "interfacial walking effect" has been reduced. These factors collectively promote overall diffusion. Notably, the diffusion rate is not positively correlated to the mesopore size. The multicomponent catalysts with smaller mesopores exhibit higher diffusion rates due to the "confinement effect." When nonzeolitic mesopores are randomly dispersed around the zeolitic component (Figure 3f-3), the likelihood of self-diffusion within nonzeolitic components increases, the re-enter into micropores and repeat the micropore diffusion process might be reduced,[54] though this effect is less significant for macromolecule guests.

To date, we have investigated the diffusion properties and microscopic mechanisms associated with various pore interconnectivities between components in the ZSM-5@meso-$SiO_2$ core−shell model multicomponent catalysts. Then, our next effort is to explore the influences from temperature. To assess the effects of different temperatures, time-resolved in situ infrared spectroscopy measurements were conducted in a range of temperatures (433, 453, 473, and 493 K) on three samples: nZ5, nZ5@S-R, and nZ5@S-P (Figure 3e). All experiments were conducted three times, and the final $\tau_{zeolite}^{-1}$ values were determined based on the averaged values and repeated errors. The repeated experiments and fitting procedure are provided in Figures S20−S22. The summary of repeated results is presented in Figure 3e and Table S4. The results indicate that the adsorption and diffusion behaviors vary significantly with the temperature. At lower temperatures (433−453 K), ZSM-5 and the two core−shell samples exhibit similar diffusion properties ($\tau_{zeolite}^{-1}$). This indicates that all mesoporous shells tend to adsorb more guest molecules at lower temperatures, which is due to the gradual loss of entropy upon collision with the roughened surface.[46] This enriched adsorption capability is also


https://doi.org/10.1021/jacs.5c00214
J. Am. Chem. Soc. 2025, 147, 18550−18562

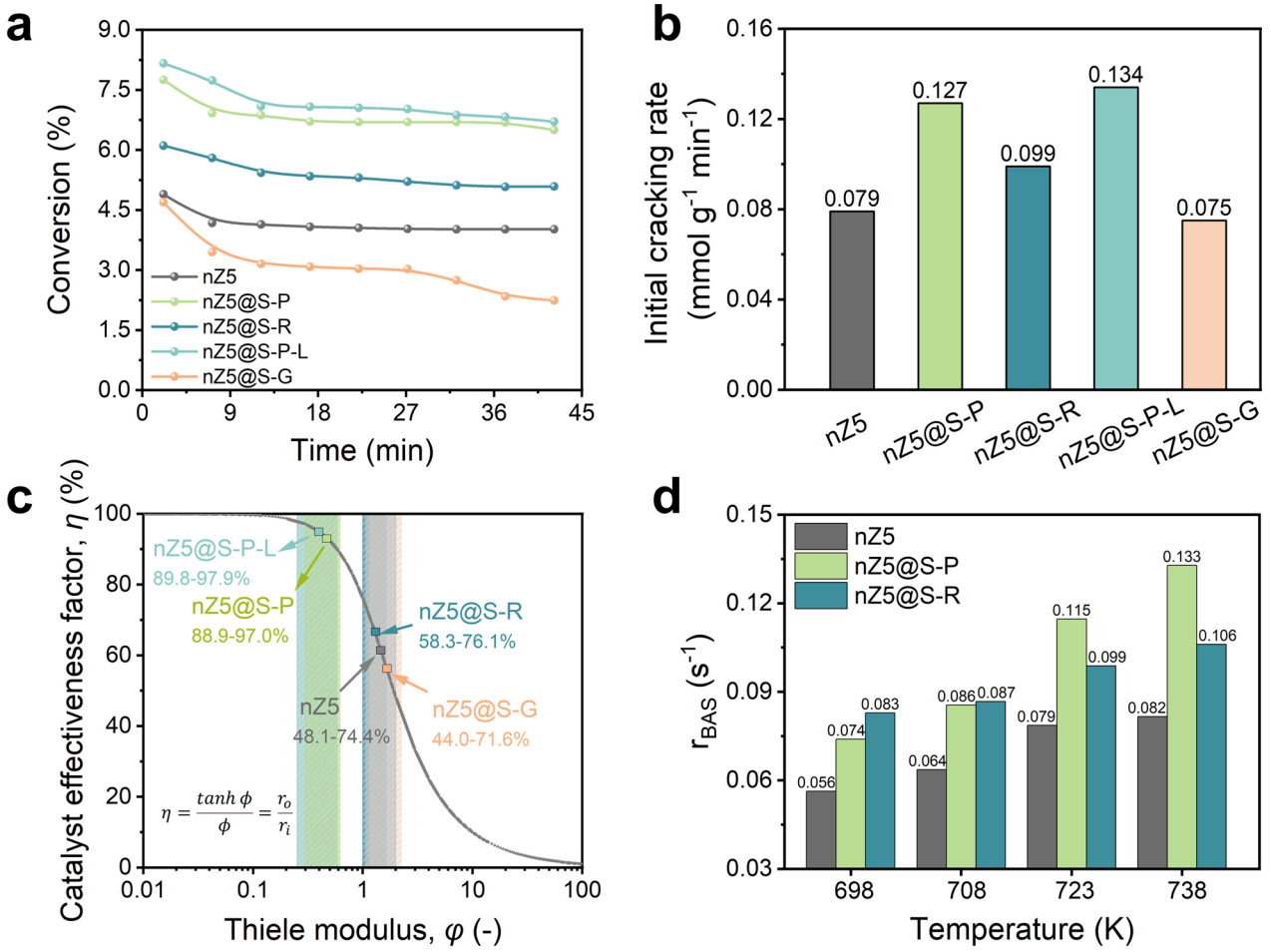


**Figure 4.** (a) Isooctane cracking conversion as a function of time on stream and (b) initial cracking rates for model catalysts. (c) Estimating Thiele modulus and catalyst effectiveness factor of model catalysts. (d) Isooctane conversion rate based on the BAS number at different temperatures.

verified by super-resolution structured illumination microscopy (SIM) using 4-(4-diethylaminostyryl-1-methylpyridiniumiodide) as a fluorescent probe to record the dynamic adsorption process over time (Figure S23). During the observation period, the fluorescence signals of the ZSM-5 sample showed no significant change, while the other two core−shell samples exhibited notable fluorescence signals, confirming that the nonzeolite mesoporous shell has an enrichment capability for adsorbing guest molecules at low temperatures. The role of mesoporous structures is more complex at high temperatures. When the temperature is high, the stuck molecules in the mesopores diffuse toward the interface and then transfer into the micropores. When the testing temperature exceeds 473 K, although the $\tau_{zeolite}^{-1}$ for all samples increases with temperature, the extent of such enhancement is quite discrepant. For nZ5@S-P, its $\tau_{zeolite}^{-1}$ value exhibits a remarkable increase, whereas the improvements for the other two samples are much lower. It means that at elevated temperatures, diffusion across the micro/mesopore interface becomes more critical. A well-connected pore orientation at the interface of the core−shell sample effectively accelerates this diffusion. Consequently, the corresponding diffusion properties are more sensitive to pore interconnectivity at high temperatures, resulting in more pronounced differences among the samples. Therefore, the diffusion property of the nZ5@S-P sample is most sensitive to temperature changes. It can be qualitatively estimated that at the reaction temperature, the influence of pore interconnectivity will be more crucial, and thus multicomponent catalysts with better connectivity will have a greater diffusion advantage at high temperatures.

For multicomponent catalytic systems where bulky reactants like polyolefins or residual oil are preconverted into intermediates via nonzeolitic components, the migrated intermediates could be varied, which may also contain isohydrocarbons and aromatics.[16] In order to explore how these intermediates with different kinetic diameters are influenced by the micro/mesopore interconnectivity, two additional probe molecules, n-octane and cumene (with kinetic diameters of 0.49 and 0.68 nm, respectively), were also selected as intermediates alongside isooctane. N-octane and cumene represent the intermediate products can easily or hard to enter the ZSM-5 micropores due to a slight or severe diffusion resistance. The time-resolved in situ FTIR technology and fitting results are presented in Figures S24 and S25, and Table S5. When small molecules like *n*-octane are adopted as the probe molecule (Figure S24, Table S5), the $\tau_{zeolite}^{-1}$ of the samples increases in the following order: nZ5 < nZ5@S-P ≈ nZ5@S-P-L < nZ5@S-R < nZ5@S-G. This infers that the influence of micro/mesopore orientation may be less significant for small molecules. The diffusion properties are more influenced by spatial distribution than by micro/mesopore orientation connectivity in multicomponent systems for small molecules. For bulky molecules such as cumene (0.68 nm), which is also a model molecule of coke precursors, its diffusion properties ($\tau_{zeolite}^{-1}$) increase in the


https://doi.org/10.1021/jacs.5c00214
J. Am. Chem. Soc. 2025, 147, 18550−18562

following order: nZ5@S-R < nZ5@S-G < nZ5 < nZ5@S-P-L < nZ5@S-P (Figure S25, Table S5), indicating that the diffusion properties of bulky molecules are significantly restricted by the micro/mesopore orientation connectivity. The diffusion is greatly restricted by the orientation connectivity of the micro/mesopores, and this diffusion behavior is generally consistent with that of isooctane, which can be of support for the diffusion of restricted bulky molecules. The specific behavior still differs slightly, possibly due to the intrinsic property differences between aromatic and aliphatic hydrocarbons. The $\pi$-electron interaction between aromatic molecules and acidic sites, as well as the rotation of the molecules, will affect diffusion. Nevertheless, samples with well-connected micro/mesopore orientation between components exhibit a significant diffusion advantage.

**Catalytic Efficiency Assessment of Multicomponent Model Catalysts in Catalytic Cracking of Model Intermediates.** To evaluate how changes in pore interconnectivity of industrial multicomponent zeolite catalysts affect their catalytic performance, the catalytic cracking performance of model intermediates, i.e., isooctane, was evaluated to quantitatively establish the structure-diffusion-reactivity relationship. The catalytic cracking was chosen as a model reaction to evaluate the catalytic performance of the ZSM-5@meso-$SiO_2$ model catalysts. Since the active components all come from ZSM-5, the selectivity of the products is not emphasized here. Considering that the isooctane conversions for some of the samples were higher than 5%, the initial apparent reaction rates (measured at 3 min after the reaction commenced) under integral reactor conditions were tested. The conversion over time and the initial rates ($r$) of the five model catalysts are presented in Figure 4a,b. For samples with a uniform and well-connected meso-$SiO_2$ shell (nZ5@S-P and nZ5@S-P-L), the initial rates were 0.122 and 0.128 mmol $g^{-1}$ $min^{-1}$, respectively. In contrast, for the samples with the meso-$SiO_2$ shell either randomly connected (nZ5@S-R) or randomly dispersed (nZ5@S-G), their initial cracking reaction rates were 0.099 and 0.075 mmol·$g^{-1}$·$min^{-1}$, respectively. In order to quantitatively correlate with diffusion properties (indexed as $\tau_{zeolite}^{-1}$) and the catalytic performance (indexed as $r$), the catalyst effectiveness factor ($\eta$) is adopted and calculated using Thiele modulus ($\phi$) as an intermediate:

$$\eta = \frac{\tanh \phi}{\phi} = \frac{r_0}{r_i}$$

where $r_0$ is the apparent reaction rate and $r_i$ is the intrinsic reaction rate. The differences in acid quantity and density among different samples have been corrected in the calculation equation (Eq S10) in the process of determining the catalyst effectiveness factor. For a detailed calculation method, see cf. Supporting Information 1.6. The catalyst effectiveness for all model catalysts is summarized in Figure 4c and Table S6 based on the two types of expression (cf. Figure S3). For the nZ5@S-R and nZ5@S-G samples, their lower $\eta$ values (approximately 44−76%) indicate that both disconnected micro/mesopore orientation and random spatial distribution can lead to strong diffusion resistance between the microporous ZSM-5 core and the mesoporous $SiO_2$ shell, severely impeding the iso-octane diffusion and its subsequent catalytic cracking reaction. Conversely, the catalyst effectiveness of the samples with well-connected core and shell orientations (nZ5@S-P and nZ5@S-P-L) can reach 89−98%. Furthermore, to exclude the effect of different acidities on the apparent catalytic activities, the apparent reaction rates per Brønsted acid site (BAS) ($r_{BAS}$) were calculated (using Eq S4) and compared in Figures 4d and S26. The effect of temperature on the apparent reaction rates for each sample is generally similar to that on the corresponding diffusion rate (Figure 3e): the apparent reaction rate is more sensitive to pore interconnectivity at high temperatures than at low temperatures. In comparison with multicomponent counterparts, it is noteworthy that the single-component nZ5 sample ($b$-oriented ZSM-5 nanosheet that serves as a model hierarchical zeolite) has a catalytic effectiveness factor of only 48−74%. Such results clearly demonstrate that the well-connected pore structure in between microporous zeolitic and mesoporous nonzeolitic components effectively reduces the diffusion resistance and enhances the catalytic efficiency of the zeolitic component for bulky reactants such as isooctane, while for samples with nonideal pore interconnectivities between zeolitic and nonzeolitic components, this improvement is not as pronounced. The findings emphasize that although constructing hierarchical zeolite materials by introducing meso- and/or macrostructures into the zeolite framework effectively improves diffusion properties and catalyst efficiency, such advantages can be fully exploited under industrial multicomponent zeolite catalysts only if the pore interconnectivity between zeolitic and nonzeolitic components is totally fulfilled.

## CONCLUSIONS

In this study, a quantitative structure-performance relationship of diffusion properties and reaction kinetics performance under controlled pore interconnectivity between zeolitic and nonzeolitic components was systematically established using ZSM-5@meso-$SiO_2$ as a model multicomponent industrial zeolite-based catalyst. HP $^{129}Xe$ NMR effectively identifies the complex pore interconnectivity and diffusion paths between zeolitic and nonzeolitic components, while time-resolved in situ infrared spectroscopy accurately distinguishes the diffusion properties of zeolitic components within multicomponent systems. Advanced characterization tools are capable of highlighting how the interface properties between zeolitic and nonzeolitic components impact both diffusion and reaction catalytic efficiency. The results reveal that nonideal pore interconnectivities between zeolitic and nonzeolitic components, which can be due to either disconnected micro/mesopore orientation, random spatial distribution, or mismatching relative pore sizes thereof, can awaken diffusion properties and reaction performances. Conversely, when the zeolitic and nonzeolitic components have well-connected micro/mesopore orientation, it can effectively accelerate interfacial diffusion and fully enhance the catalytic efficiency of the zeolitic component. Therefore, introducing hierarchical structures into the zeolite alone does not sufficiently enhance diffusion and catalyst efficiency under industrial multicomponent conditions. The diffusivities of zeolite-based catalysts under industrial catalysis circumstances are strongly determined by high levels of pore systems' connectivity so that molecules can effectively diffuse into and out of the zeolitic components. For the elaborate design of industrial multicomponent catalysts, more attention should be devoted to constructing highly interconnected hierarchical pore systems between zeolitic and nonzeolitic components (both intra- and intercrystal spaces) and their surface properties. Finally, revealing the transport properties in these complex pore systems of practical zeolitic catalysts is unambiguously vital to guiding the design of high-performance practical catalysts.


https://doi.org/10.1021/jacs.5c00214
J. Am. Chem. Soc. 2025, 147, 18550−18562

However, there is still a long way to go to achieve a comprehensive acidity-diffusion coupling model between zeolitic and nonzeolite components and their consequences on diffusion and catalyst efficiency, especially when directly relying on a real industrial catalyst. This presents a significant challenge for interfacial characterization techniques. Furthermore, other zeolitic and nonzeolitic components interactions that exist in practical catalysts, such as aluminum migration and interfacial modifications, require further in-depth investigation in future studies.

## ■ ASSOCIATED CONTENT

### Supporting Information

The Supporting Information is available free of charge at https://pubs.acs.org/doi/10.1021/jacs.5c00214.

Additional details of experimental procedures, sample preparation, catalyst characterization, continuous-flow hyperpolarized $^{129}$Xe NMR experiment, uptake rate measurements of diffusion catalytic tests, and calculation of catalyst effectiveness factor; XRD, SAXS, SEM, TEM, $NH_3$-TPD, NMR, iDPC-STEM, STEM-mapping, and HP $^{129}$Xe NMR; repeated uptake experiments and error bounds; SIM experiments; *n*-octane and cumene uptake experiments; conversion correlation experiments; characterization data; diffusion time constants; Thiele modulus; and catalyst effectiveness factor estimation (PDF)

## ■ AUTHOR INFORMATION


### Corresponding Authors

**Peng Peng** − *State Key Laboratory of Heavy Oil Processing, School of Chemistry and Chemical Engineering, China University of Petroleum (East China), Qingdao 266580, P. R. China; Interdisciplinary Institute of NMR and Molecular Sciences, Hubei Province for Coal Conversion and New Carbon Materials, School of Chemistry and Chemical Engineering, Wuhan University of Science and Technology, Wuhan 430081, P. R. China;* orcid.org/0000-0002-8258-6812; Email: peng.peng@wust.edu.cn

**Zifeng Yan** − *State Key Laboratory of Heavy Oil Processing, School of Chemistry and Chemical Engineering, China University of Petroleum (East China), Qingdao 266580, P. R. China;* orcid.org/0000-0002-9215-3842; Email: zfyancat@upc.edu.cn

**Shutao Xu** − *National Engineering Research Center of Lower-Carbon Catalysis Technology and State Key Laboratory of Catalysis, Dalian Institute of Chemical Physics, Chinese Academy of Sciences, Dalian 116023, P. R. China; University of Chinese Academy of Sciences, Beijing 100049, P. R. China;* orcid.org/0000-0003-4722-8371; Email: xushutao@dicp.ac.cn

### Authors

**Yipu Xu** − *State Key Laboratory of Heavy Oil Processing, School of Chemistry and Chemical Engineering, China University of Petroleum (East China), Qingdao 266580, P. R. China; National Engineering Research Center of Lower-Carbon Catalysis Technology, Dalian Institute of Chemical Physics, Chinese Academy of Sciences, Dalian 116023, P. R. China*

**Hanlixin Wang** − *CAS Key Laboratory of Separation Science for Analytical Chemistry, Dalian Institute of Chemical Physics, Chinese Academy of Sciences, Dalian 116023, P. R. China; University of Chinese Academy of Sciences, Beijing 100049, P. R. China*

**Hao Xiong** − *Engineering and Technology, Department of Chemical Engineering, Tsinghua University, Beijing 100084, P. R. China*

**Zhaochao Xu** − *CAS Key Laboratory of Separation Science for Analytical Chemistry, Dalian Institute of Chemical Physics, Chinese Academy of Sciences, Dalian 116023, P. R. China; University of Chinese Academy of Sciences, Beijing 100049, P. R. China;* orcid.org/0000-0002-2491-8938

**Xiao Chen** − *Engineering and Technology, Department of Chemical Engineering, Tsinghua University, Beijing 100084, P. R. China*

**Yanpeng Li** − *State Key Laboratory of Heavy Oil Processing, School of Chemistry and Chemical Engineering, China University of Petroleum (East China), Qingdao 266580, P. R. China*

**Anmin Zheng** − *Interdisciplinary Institute of NMR and Molecular Sciences, Hubei Province for Coal Conversion and New Carbon Materials, School of Chemistry and Chemical Engineering, Wuhan University of Science and Technology, Wuhan 430081, P. R. China*

**Yingxu Wei** − *National Engineering Research Center of Lower-Carbon Catalysis Technology and State Key Laboratory of Catalysis, Dalian Institute of Chemical Physics, Chinese Academy of Sciences, Dalian 116023, P. R. China; University of Chinese Academy of Sciences, Beijing 100049, P. R. China;* orcid.org/0000-0002-0412-1980

**Zhongmin Liu** − *National Engineering Research Center of Lower-Carbon Catalysis Technology and State Key Laboratory of Catalysis, Dalian Institute of Chemical Physics, Chinese Academy of Sciences, Dalian 116023, P. R. China; University of Chinese Academy of Sciences, Beijing 100049, P. R. China;* orcid.org/0000-0002-7999-2940

Complete contact information is available at: https://pubs.acs.org/10.1021/jacs.5c00214


### Author Contributions

This manuscript was written through contribution of all authors. All authors have given approval to the final version of the manuscript.

### Notes

The authors declare no competing financial interest.

## ■ ACKNOWLEDGMENTS

This work was supported by the National Science Foundation of China (22241801; 22288101; 22022202; 22032005; 21991090; 21991092; 21991093; 22302230; and 22372197), the Dalian Outstanding Young Scientist Foundation (2021RJ01), the Liaoning International Joint Laboratory Project (2024JH2/102100005), the PetroChina (KYWX-22-017; KYWX-22-012), the Postdoctoral Fellowship Program of CPSF (GZC20241291), the State Key Laboratory of Heavy Oil Processing (SKLHOP202402007), the Innovation fund project for graduate student of China University of Petroleum (East China), the Fundamental Research Funds for the Central Universities (no. 24CX04004A), the Hubei Provincial Natural Science Foundation of China (2025AFA008), the Natural Science Foundation of Wuhan (2024040701010058), and the Shandong Provincial Natural Science Foundation of China (ZR2021QB082).

## REFERENCES


(1) Vogt, E. T.; Weckhuysen, B. M. Fluid catalytic cracking: recent developments on the grand old lady of zeolite catalysis. *Chem. Soc. Rev.* **2015**, *44*, 7342−7370.

(2) Velty, A.; Corma, A. Advanced zeolite and ordered mesoporous silica-based catalysts for the conversion of $CO_2$ to chemicals and fuels. *Chem. Soc. Rev.* **2023**, *52*, 1773−1946.

(3) Li, Y.; Yu, J. Emerging applications of zeolites in catalysis, separation and host-guest assembly. *Nat. Rev. Mater.* **2021**, *6*, 1156−1174.

(4) Fu, D.; Park, Y.; Davis, M. E. Confinement effects facilitate low-concentration carbon dioxide capture with zeolites. *Proc. Natl. Acad. Sci. U. S. A.* **2022**, *119*, No. e2211544119.

(5) Chi, X.; Li, M.; Di, J.; Bai, P.; Song, L.; Wang, X.; Li, F.; Liang, S.; Xu, J.; Yu, J. A highly stable and flexible zeolite electrolyte solid-state Li-air battery. *Nature* **2021**, *592*, 551−557.

(6) Tai, W. S.; Dai, W. J.; Wu, G. J.; Li, L. D. A simple strategy for synthesis of b-axis-oriented MFI zeolite macro-nanosheets. *Chem. Synth.* **2023**, *3*, 38.

(7) Peng, P.; Gao, X. H.; Yan, Z. F.; Mintova, S. Diffusion and catalyst efficiency in hierarchical zeolite catalysts. *Natl. Sci. Rev.* **2020**, *7*, 1726−1742.

(8) Lu, P.; Xu, J.; Sun, Y.; Guillet-Nicolas, R.; Willhammar, T.; Fahda, M.; Dib, E.; Wang, B.; Qin, Z.; Xu, H.; Cho, J.; Liu, Z.; Yu, H.; Yang, X.; Lang, Q.; Mintova, S.; Zou, X.; Valtchev, V. A stable zeolite with atomically ordered and interconnected mesopore channel. *Nature* **2024**, *636*, 368−373.

(9) Lee, S.; Park, Y.; Choi, M. Cooperative Interplay of Micropores/Mesopores of Hierarchical Zeolite in Chemical Production. *ACS Catal.* **2024**, *14*, 2031−2048.

(10) Yang, X. Y.; Chen, L. H.; Li, Y.; Rooke, J. C.; Sanchez, C.; Su, B. L. Hierarchically porous materials: synthesis strategies and structure design. *Chem. Soc. Rev.* **2017**, *46*, 481−558.

(11) Mitchell, S.; Michels, N. L.; Perez-Ramirez, J. From powder to technical body: the undervalued science of catalyst scale up. *Chem. Soc. Rev.* **2013**, *42*, 6094−6112.

(12) Yang, K.; Zhang, D.; Zou, M.; Yu, L.; Huang, S. The known and overlooked sides of zeolite-extrudate catalysts. *ChemCatChem.* **2021**, *13*, 1414−1423.

(13) Kennes, K.; Kubarev, A.; Demaret, C.; Treps, L.; Delpoux, O.; Rivallan, M.; Guillon, E.; Méthivier, A.; de Bruin, T.; Gomez, A.; Harbuzaru, B.; Roeffaers, M. B. J.; Chizallet, C. Multiscale visualization and quantification of the effect of binders on the acidity of shaped zeolites. *ACS Catal.* **2022**, *12*, 6794−6808.

(14) Whiting, G. T.; Chung, S.-H.; Stosic, D.; Chowdhury, A. D.; van der Wal, L. I.; Fu, D.; Zecevic, J.; Travert, A.; Houben, K.; Baldus, M.; Weckhuysen, B. M. Multiscale mechanistic insights of shaped catalyst body formulations and their impact on catalytic properties. *ACS Catal.* **2019**, *9*, 4792−4803.

(15) Vollmer, I.; Jenks, M. J. F.; Mayorga Gonzalez, R.; Meirer, F.; Weckhuysen, B. M. Plastic waste conversion over a refinery waste catalyst. *Angew. Chem., Int. Ed.* **2021**, *60*, 16101−16108.

(16) Zhang, Y.; Wang, J.; Xie, X.; Wang, X.; Wu, W. D.; Chen, X. D.; Wu, Z. Deep cracking of bulky hydrocarbons into light products via tandem catalysis over uniform interconnected ZSM-5@AlSBA-15 Composites. *Small* **2024**, *20*, No. 2309114.

(17) Liu, S. B.; Kots, P. A.; Vance, B. C.; Danielson, A.; Vlachos, D. G. Plastic waste to fuels by hydrocracking at mild conditions. *Sci. Adv.* **2021**, *7*, No. eabf8283.

(18) Wang, B.; Han, C.; Zhang, Q.; Li, C.; Yang, C.; Shan, H. Studies on the preliminary cracking of heavy oils: the effect of matrix acidity and a proposal of a new reaction route. *Energy Fuels* **2015**, *29*, 5701−5713.

(19) Duan, J.; Chen, W.; Wang, C.; Wang, L.; Liu, Z.; Yi, X.; Fang, W.; Wang, H.; Wei, H.; Xu, S.; Yang, Y.; Yang, Q.; Bao, Z.; Zhang, Z.; Ren, Q.; Zhou, H.; Qin, X.; Zheng, A.; Xiao, F. S. Coking-resistant polyethylene upcycling modulated by zeolite micropore diffusion. *J. Am. Chem. Soc.* **2022**, *144*, 14269−14277.

(20) Hu, S.; Liu, J.; Ye, G.; Zhou, X.; Coppens, M. O.; Yuan, W. Effect of external surface diffusion barriers on platinum/Beta-catalyzed isomerization of n-pentane. *Angew. Chem., Int. Ed.* **2021**, *60*, 14394−14398.

(21) Zhou, J.; Fan, W.; Wang, Y. D.; Xie, Z. K. The essential mass transfer step in hierarchical/nano zeolite: Surface diffusion. *Natl. Sci. Rev.* **2020**, *7*, 1630−1632.

(22) Qi, X.; Vattipalli, V.; Zhang, K.; Bai, P.; Dauenhauer, P. J.; Fan, W. Adsorptive nature of surface barriers in MFI nanocrystals. *Langmuir* **2019**, *35*, 12407−12417.

(23) Qin, Y.; Gao, X.; Zhang, H.; Zhang, S.; Zheng, L.; Li, Q.; Mo, Z.; Duan, L.; Zhang, X.; Song, L. Measurements and distinguishment of mass transfer processes in fluid catalytic cracking catalyst particles by uptake and frequency response methods. *Catal. Today* **2015**, *245*, 147−154.

(24) Peng, P.; Stosic, D.; Aitblal, A.; Vimont, A.; Bazin, P.; Liu, X.-M.; Yan, Z.-F.; Mintova, S.; Travert, A. Unraveling the diffusion properties of zeolite-based multicomponent catalyst by combined gravimetric analysis and IR spectroscopy (AGIR). *ACS Catal.* **2020**, *10*, 6822−6830.

(25) Hargreaves, J. S. J.; Munnoch, A. L. A survey of the influence of binders in zeolite catalysis. *Catalysis Science & Technology* **2013**, *3*, 1165.

(26) Zhang, K.; Jiang, X.; Forte, M. J.; Sun, M.; AlAbdullah, M.; AlAmer, M.; Aljishi, M.; AlSayed, E.; AlSadat, W.; Gates, B. C.; Katz, A. Influence of binders and matrices on zeolite-containing catalysts. *Catalysis Science & Technology* **2024**, *14*, 4740−4755.

(27) Zeng, S.; Xu, S.; Gao, S.; Gao, M.; Zhang, W.; Wei, Y.; Liu, Z. Differentiating diffusivity in different channels of ZSM-5 zeolite by pulsed field gradient (PFG) NMR. *ChemCatChem.* **2020**, *12*, 463−468.

(28) Zhang, J.; Ren, L.; Zhang, A.; Guo, X.; Song, C. MFI nanosheets: a rising star in zeolite materials. *Mater. Chem. Front.* **2024**, *8*, 595−602.

(29) Kärger, J.; Avramovska, M.; Freude, D.; Haase, J.; Hwang, S.; Valiullin, R. Pulsed field gradient NMR diffusion measurement in nanoporous materials. *Adsorption* **2021**, *27*, 453−484.

(30) Qian, X. F.; Li, B.; Hu, Y. Y.; Niu, G. X.; Zhang, D. Y.; Che, R. C.; Tang, Y.; Su, D. S.; Asiri, A. M.; Zhao, D. Y. Exploring meso-/microporous composite molecular sieves with core-shell structures. *Chem.—Eur. J.* **2012**, *18*, 931−939.

(31) Stöber, W.; Fink, A.; Bohn, E. Controlled growth of monodisperse silica spheres in the micron size range. *J. Colloid Interface Sci.* **1968**, *26*, 62−69.

(32) LaMer, V. K.; Dinegar, R. H. Theory, production and mechanism of formation of monodispersed hydrosols. *J. Am. Chem. Soc.* **1950**, *72*, 4847−4854.

(33) Cychosz, K. A.; Guillet-Nicolas, R.; García-Martínez, J.; Thommes, M. Recent advances in the textural characterization of hierarchically structured nanoporous materials. *Chem. Soc. Rev.* **2017**, *46*, 389−414.

(34) Wisser, D.; Hartmann, M. $^{129}$Xe NMR on porous materials: basic principles and recent applications. *Adv. Mater. Interfaces* **2020**, *8*, 200126.

(35) Weiland, E.; Springuel-Huet, M.-A.; Nossov, A.; Gedeon, A. $^{129}$Xenon NMR: Review of recent insights into porous materials. *Microporous Mesoporous Mater.* **2016**, *225*, 41−65.

(36) Bonardet, J.-L.; Fraissard, J.; Gédéon, A.; Springuel-Huet, M.-A. Nuclear magnetic resonance of physisorbed $^{129}$Xe used as a probe to investigate porous solids. *Catal. Rev.-Sci. Eng.* **1999**, *41*, 115−225.

(37) Liu, Y.; Zhang, W. P.; Han, X. W.; Bao, X. H. Hyperpolarized $^{129}$Xe NMR and its applications in characterization of porous catalytic materials. *Chin. J. Catal.* **2006**, *27*, 827−836.

(38) Liu, Y.; Zhang, W. P.; Liu, Z. C.; Xu, S. T.; Wang, Y. D.; Xie, Z. K.; Han, X. W.; Bao, X. H. Direct observation of the mesopores in ZSM-5 zeolites with hierarchical porous structures by laser-hyperpolarized $^{129}$Xe NMR. *J. Phys. Chem. C* **2008**, *112*, 15375−15381.

(39) Led, J. J.; Gesmar, H. The applicability of the magnetization-transfer NMR technique to determine chemical exchange rates in extreme cases. The importance of complementary experiments. *J. Magn. Reson.* **1969**, *49*, 444−463.

(40) Leigh, J. S., Jr Relaxation times in systems with chemical exchange: Some exact solutions. *J. Magn. Reson.* **1969**, *4*, 308−311.




https://doi.org/10.1021/jacs.5c00214
J. Am. Chem. Soc. 2025, 147, 18550−18562

(41) Schneider, D.; Kondrashova, D.; Valiullin, R.; Bunde, A.; Kärger, J. Mesopore-promoted transport in microporous materials. *Chem. Ing. Technol.* **2015**, *87*, 1794−1809.
(42) Bai, P.; Haldoupis, E.; Dauenhauer, P. J.; Tsapatsis, M.; Siepmann, J. I. Understanding diffusion in hierarchical zeolites with house-of-cards nanosheets. *ACS Nano* **2016**, *10*, 7612−7618.
(43) Hwang, S.; Kärger, J. NMR diffusometry with guest molecules in nanoporous materials. *Magn. Reson. Imaging* **2019**, *56*, 3−13.
(44) Sun, M.-H.; Zhou, J.; Hu, Z.-Y.; Chen, L.-H.; Li, L.-Y.; Wang, Y.-D.; Xie, Z.-K.; Turner, S.; Van Tendeloo, G.; Hasan, T.; Su, B.-L. Hierarchical zeolite single-crystal reactor for excellent catalytic efficiency. *Matter* **2020**, *3*, 1226−1245.
(45) Yuan, J.; Gao, M.; Liu, Z.; Tang, X.; Tian, Y.; Ma, G.; Ye, M.; Zheng, A. Hyperloop-like diffusion of long-chain molecules under confinement. *Nat. Commun.* **2023**, *14*, 1735.
(46) Reitmeier, S. J.; Gobin, O. C.; Jentys, A.; Lercher, J. A. Enhancement of sorption processes in the zeolite H-ZSM5 by postsynthetic surface modification. *Angew. Chem., Int. Ed.* **2009**, *48*, 533−538.
(47) Dong, Z.; Chen, W.; Xu, K.; Liu, Y.; Wu, J.; Zhang, F. Understanding the structure-activity relationships in catalytic conversion of polyolefin plastics by zeolite-based catalysts: A critical review. *ACS Catal.* **2022**, *12*, 14882−14901.
(48) Bonilla, M.; Titze, T.; Schmidt, F.; Mehlhorn, D.; Chmelik, C.; Valiullin, R.; Bhatia, S.; Kaskel, S.; Ryoo, R.; Kärger, J. Diffusion study by IR micro-imaging of molecular uptake and release on mesoporous zeolites of structure type CHA and LTA. *Materials* **2013**, *6*, 2662−2688.
(49) Hwang, S.; Kärger, J.; Miersemann, E. Diffusion and reaction in pore hierarchies by the two-region model. *Adsorption* **2021**, *27*, 761−776.
(50) Hwang, S.; Schneider, D.; Haase, J.; Miersemann, E.; Kärger, J. Quantifying diffusion-limited catalytic reactions in hierarchically structured porous materials by combining kinetic monte carlo simulations with the two-region model of diffusion. *ChemCatChem* **2022**, *14*, No. e202200829.
(51) Sun, M. H.; Gao, S. S.; Hu, Z. Y.; Barakat, T.; Liu, Z.; Yu, S.; Lyu, J. M.; Li, Y.; Xu, S. T.; Chen, L. H.; Su, B. L. Boosting molecular diffusion following the generalized Murray's Law by constructing hierarchical zeolites for maximized catalytic activity. *Natl. Sci. Rev.* **2022**, *9*, No. nwac236.
(52) Peng, Z.; Chen, L.-H.; Sun, M.-H.; Zhao, H.; Wang, Z.; Li, Y.; Li, L.-Y.; Zhou, J.; Liu, Z.-C.; Su, B.-L. A hierarchical zeolitic Murray material with a mass transfer advantage promotes catalytic efficiency improvement. *Inorg. Chem. Front.* **2018**, *5*, 2829−2835.
(53) Liu, X.; Wang, C.; Zhou, J.; Liu, C.; Liu, Z.; Shi, J.; Wang, Y.; Teng, J.; Xie, Z. Molecular transport in zeolite catalysts: depicting an integrated picture from macroscopic to microscopic scales. *Chem. Soc. Rev.* **2022**, *51*, 8174−8200.
(54) Qi, X.; Vattipalli, V.; Dauenhauer, P. J.; Fan, W. Silica nanoparticle mass transfer fins for MFI composite materials. *Chem. Mater.* **2018**, *30*, 2353−2361.


https://doi.org/10.1021/jacs.5c00214
*J. Am. Chem. Soc.* 2025, 147, 18550−18562